Journal of Scientific Computing (2021) 89:29
https://doi.org/10.1007/s10915-021-01635-4

Time Step Restrictions for Strong-Stability-Preserving Multistep Runge–Kutta Discontinuous Galerkin Methods

Benjamin Yeager[1] · **Ethan Kubatko**[2] · **Dylan Wood**[3]

Received: 16 August 2020 / Revised: 24 March 2021 / Accepted: 24 April 2021 /
Published online: 17 September 2021

Abstract
Discontinuous Galerkin finite element spatial discretizations are often used in a method-of-lines approach with an ordinary differential equation solver to step the solution forward in time. Explicit strong-stability-preserving time steppers are a popular choice because they provably preserve the nonlinear stability properties of the forward Euler method applied to discontinuous Galerkin semi-discretized equations, subject to a time step constraint. While nonlinear stability is guaranteed by strong-stability-preservation, a separate condition for linear stability of the combined scheme must also be satisfied. In this work, we assess the linear stability properties of discontinuous Galerkin spatial discretizations with a set of strong-stability-preserving multistep Runge–Kutta methods. We find that, in all cases, the constraint for linear stability is more strict than that for strong-stability-preservation. For each order, from the set of multistep Runge–Kutta methods, we select an optimal time stepper that requires the fewest evaluations of the discontinuous Galerkin operator. All methods are tested for convergence in application to both a linear and a nonlinear partial differential equation, and all methods are found to converge in both cases using the maximum stable time step as determined by the stability constraints found in this paper.

Keywords Discontinuous Galerkin · Strong-stability-preserving · Multistep Runge–Kutta · Linear stability · Time stepping

Mathematics Subject Classification 65M12 · 65M60

1 Introduction

Discontinuous Galerkin (DG) finite element spatial discretizations are often paired with explicit time steppers in a method-of-lines approach for the numerical solution of hyperbolic conservation laws. Among the most widely used approaches of this type are the Runge–Kutta

✉ Benjamin Yeager
by16@nyu.edu

[1] New York University, New York, USA

[2] The Ohio State University, Columbus, OH, USA

[3] Notre Dame University, South Bend, IN, USA

(RK) DG methods originally developed by Cockburn and Shu (et al) in a series of articles that progresses from one-dimensional, scalar conservation laws to multidimensional systems of conservations laws [8–12]. These methods have been further developed, analyzed and applied by a number of authors for a wide variety of problems; see, for example, [7,17,21,25–28]. One of the oft-cited advantages of using DG spatial discretizations is the (relative) ease and efficiency with which high-order spatial accuracy can be achieved via the use of high-degree piecewise polynomials. Unlike high-order finite difference and essentially non-oscillatory (ENO)-type spatial discretizations, this high-order spatial accuracy is achieved without an increase in stencil width and, when paired with explicit time steppers, results in a fully discrete scheme with an extremely local data structure (specifically, elements only require information from immediate neighbors regardless of the order of accuracy). This, in turn, gives rise to embarrassingly high parallel efficiency; see, for example, [3].

Of course, it is important to point out that in order to render the resulting (fully discrete) schemes high-order accurate, high-order time stepping methods that match (or exceed) the order of accuracy of the spatial discretization must be used (where "order of accuracy" is in the sense of local truncation errors, see [12]). Furthermore, proof that the RKDG methods are total variation diminishing (TVD) (that is, that they statisfy a maximum principle in spatial dimensions, $d > 1$, see [8]) relies on the use of a special class of explicit time steppers known as strong-stability-preserving (SSP) methods (originally referred to as TVD time stepping methods; see [24]). These two facts have an important implication with regard to the overall order of accuracy that can be achieved using RKDG methods. Specifically, given that (positive coefficient) SSP RK methods have a well-known order barrier of four (see, for example, [15]), RKDG methods are, in effect, limited to fourth-order accuracy, despite the ease with which high-degree polynomials may be used in the DG spatial discretization. (We note that in practice the classic second- or third-order SSP RK method is often paired with DG spatial discretizations of order ≥ 4 to demonstrate higher-order convergence by using sufficiently "small" time steps for short durations of time so that time discretization errors do not dominate; see, for example, [1,6,14,18,22]).

However, the favorable properties of RKDG methods, in particular the proven TVD properties, can be carried over to any explicit time stepping method (under suitable time step restrictions) that can be written as a convex combination of forward Euler steps; see sections 2.2–2.5 of [13]. This is the defining feature of explicit SSP time steppers. Therefore, in this paper, we investigate pairing higher-order SSP multistep Runge–Kutta (MSRK) methods with DG spatial discretizations as a means of surpassing the fourth-order barrier of RKDG methods while retaining their favorable properties. Specifically, using the SSP MSRK methods recently developed and reported in [4], we formulate and investigate MSRKDG methods up to order ten—that is, DG spatial discretizations of degree $p = q - 1$ paired with MSRK of order q for $q = 2, 3, \ldots, 10$—where the MSRK methods have up to twenty stages and six steps.

The resulting MSRKDG methods must, of course, satisfy certain time step restrictions in order to maintain both the aforementioned TVD property, which is dictated by the so-called SSP coefficients of the time steppers (see Sect. 3), and linear stability, which is dictated by the region of absolute stability of the time stepper and the (scaled) spectral radius of the DG spatial operator (see Sect. 4). We determine these time step restrictions for the given MSRK methods and identify the most efficient pairing for a given order. The efficiency of the pairing is determined by the stricter of the two stability conditions, which in all cases investigated is the linear stability condition, *and* the number of stages used in the time stepping method, which dictates the number of times the DG spatial operator (see Eq. (5) of Sect. 2) must

be evaluated per timestep. Our numerical results demonstrate the high-order accuracy of the resulting MSRKDG schemes under our determined conditions for linear stability.

The rest of this paper is organized as follows. In the next section, the DG spatial discretization of a general, one-dimensional hyperbolic conservation law is presented. Following this, the stability conditions for the semidiscrete DG equations paired with the forward Euler (FE) and MSRK methods are discussed in Sects. 3 and 4, respectively. Section 5 provides an overview of the methods employed to determine the linear stability conditions for the MSRKDG methods, and Sect. 6 presents results from a set of numerical test cases that verify these linear stability conditions and demonstrate the stability, order of accuracy and efficiency of the MSRKDG methods. In Sect. 7, we test the convergence of MSRKDG schemes in application to both a linear and nonlinear problem using the time step restrictions presented in Sect. 6. Finally, in Sect. 8, conclusions are drawn and future work in this area is proposed.

2 The Discontinuous Galerkin Finite Element Discretization

Consider a general hyperbolic conservation law in one dimension:

$$\frac{\partial u}{\partial t} + \frac{\partial}{\partial x} f(u) = 0\,, \tag{1}$$

where $x \in \Omega = [x_L, x_R]$ is the spatial coordinate and $t \in [t_0, T]$ is time, with periodic boundary conditions $u(x_L, t) = u(x_R, t)$, and intial condition $u(x, t_0) = u_0(x)$. The function $f(u)$ is referred to as the flux function.

To begin spatial discretization of (1), we first define a partition

$$\mathcal{T}_h = \{\Omega_j \subset \Omega : \Omega_j = (x_j, x_{j+1}), \forall j = 1, 2, \ldots, N\}$$

where N is the number of elements Ω_j in the partition, and coordinates $x_1 = x_L, x_{N+1} = x_R$, and $x_j < x_{j+1}$ for all j, with the mesh spacing given by $h_j = x_{j+1} - x_j$. We can then construct the weak form of (1) over the partitioned domain by multiplying by a sufficiently smooth test function v and integrating over each element Ω_j, giving

$$\int_{\Omega_j} \frac{\partial u}{\partial t} v \, dx - \int_{\Omega_j} f\,(u)\, \frac{\partial v}{\partial x}\, dx + f(u)v\Big|_{x_j}^{x_{j+1}} = 0\,, \quad \forall\, \Omega_j \in \mathcal{T}_h, \tag{2}$$

where the second term has been integrated by parts.

Given the weak form (2), we can now define the DG piece-wise polynomial approximation of the solution by replacing u and v with $u_h^p, v_h^p \in \mathbb{V}_h^p$ where $\mathbb{V}_h^p = \{w : w \in \mathbb{P}^p(\Omega_j), \forall \Omega_j \in \mathcal{T}_h\}$ and $\mathbb{P}^p(\Omega_j)$ is the space of polynomials of degree at most $p \geq 0$ defined over the element Ω_j. Note that, because continuity of u_h^p across element boundaries is not enforced, the flux $f(u_h^p)$ at those points is not well-defined. Therefore, a numerical flux estimate $\hat{f}_j = \hat{f}(u_j^-, u_j^+)$ must be introduced in the boundary term, where

$$u_j^- = \lim_{x \to x_j^-} u_h^p(x, t) \quad \text{and} \quad u_j^+ = \lim_{x \to x_j^+} u_h^p(x, t)$$

are the values of u_h^p when approaching x_j from the left and right, respectively; see Fig. 1. Substituting u_h^p, v_h^p, and $\hat{f}_j$ for u, v and $f(u)\big|_{x_j}$, respectively, in (2), the DG-semi-discretized

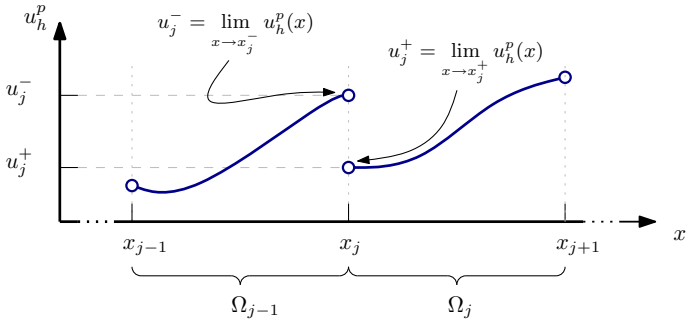

Fig. 1 Illustration of element and element boundary subscripts showing an example of a discontinuity at the boundary of two elements. In order to obtain a numerical estimate of the flux at the element boundaries, we define u_j^- as the limit of u_h^p approaching x_j from the left and u_j^+ as the limit of u_h^p approaching x_j from the right

system of equations is given by

$$\int_{\Omega_j} \frac{\partial u_h^p}{\partial t} v_h^p \, dx = \int_{\Omega_j} f_j \frac{\partial v_h^p}{\partial x} \, dx - \hat{f}_{j+1} v_h^p(x_{j+1}^-) + \hat{f}_j v_h^p(x_j^+) = 0 \,, \quad \forall \, \Omega_j \in \mathcal{T}_h. \tag{3}$$

Note that we have moved all spatial derivative terms to the right hand side and abbreviated $f(u_h^p)\big|_{\Omega_j}$ as f_j.

Next, we choose a polynomial basis $\boldsymbol{\Phi}_j = [\phi_{j1}, \phi_{j2}, \ldots, \phi_{jK}]^T$ consisting of K basis polynomials for each subspace $\mathbb{P}^p(\Omega_j)$, allowing us to write the piece-wise polynomial approximations u_h^p and v_h^p as

$$u_h^p\Big|_{\Omega_j} = \mathbf{u}_j \boldsymbol{\Phi}_j = \sum_{k=1}^{K} u_{jk}(t)\phi_{jk}(x) \quad \text{and} \quad v_h^p\Big|_{\Omega_j} = \mathbf{v}_j \boldsymbol{\Phi}_j = \sum_{l=1}^{K} v_{jl}(t)\phi_{jl}(x),$$

where $\mathbf{u}_j = [u_{j1}, u_{j2}, \ldots, u_{jK}]$ and $\mathbf{v}_j = [v_{j1}, v_{j2}, \ldots, v_{jK}]$. We refer to the time-dependent coefficients u_{jk} as the degrees of freedom of u_h^p. Note that, when the above representation of v_h^p is substituted into (3), the arbitrary constants v_{jl} cancel out.

Incorporating the above representation of u_h^p and v_h^p into (3), the DG-semi-discretized system of equations can be written in the vectorized form

$$\mathbf{M}\frac{d\mathbf{u}}{dt} = \mathbf{F}(\mathbf{u})$$

where the degrees of freedom of u_h^p have been organized in the vector $\mathbf{u} = [\mathbf{u}_1, \mathbf{u}_2, \ldots \mathbf{u}_N]^T$. The mass matrix $\mathbf{M}$ is a diagonal matrix with $K \times K$ components $\mathbf{M}_j$ given by

$$\mathbf{M}_{j,kl} = \int_{\Omega_j} \phi_{jk}\phi_{jl} \, dx \tag{4}$$

and $\mathbf{F}$ is a column vector of right-hand-side evaluations with $1 \times K$ components $\mathbf{F}_j(u_h^p)$ given by

$$\mathbf{F}_j = [F_{j1}, F_{j2}, \ldots, F_{jK}]^T$$

where

$$F_{j,l} = \int_{\Omega_j} f_j \frac{\partial \phi_{j,l}}{\partial x}\, dx - \hat{f}_{j+1}\phi_{j,l}(x_{j+1}^-) + \hat{f}_j \phi_{j,l}(x_j^+)\,.$$

Inverting the constant-in-time mass matrix, we can write the system of equations in the concise form

$$\frac{d\mathbf{u}}{dt} = \mathbf{L}\,(\mathbf{u})\ , \tag{5}$$

where the DG spatial operator $\mathbf{L}(\mathbf{u})$ is given by

$$\mathbf{L}(\mathbf{u}) = \left[\mathbf{M}_1^{-1}\mathbf{F}_1\,,\ \mathbf{M}_2^{-1}\mathbf{F}_2\,, \ldots\right]^T\ .$$

3 On the Stability of DG Method-of-Lines Schemes

After performing the DG discretization in space to obtain a system of ordinary differential equations (ODEs) (5), all that remains is to choose an ODE solver to step the solution forward in time. In the interest of maintaining the local nature of the DG discretization, we choose to limit ourselves to explicit time stepping schemes. As a first step, it is instructive to consider forward Euler time (FE) stepping. Applying the FE method to (5) with a time step size Δt, we have

$$\mathbf{u}^{n+1} = \mathbf{u}^n + \Delta t \mathbf{L}(\mathbf{u}^n)\,,$$

where $\mathbf{u}^n = \mathbf{u}(n\Delta t)$. Recall that, in addition to the typical requirements for linear stability, we seek a scheme that is also TVD.

It has been shown that the DG semi-discretized system of equations with an appropriate slope limiter and FE time stepping is TVD under the condition

$$\Delta t \le \Delta t_{\text{FE}} = \frac{\min_j(h_j)}{2(K_1 + K_2)}\,, \tag{6}$$

where K_1 and K_2 are the Lipschitz constants of $\hat{f}$ with respect to the first and second arguments, respectively; see, for example, [13]. In the case of a linear flux function $f = cu$ with $c > 0$, with the use of an upwind numerical flux and uniform mesh spacing $\Delta x = h_j$ for all j, (6) yields the following condition for a TVD combined scheme:

$$|c|\frac{\Delta t}{\Delta x} \le \frac{1}{2}\,.$$

However, von Neumann stability analysis shows that the DG semi-discretized equations with the FE time stepper are unconditionally linearly unstable for constant $\Delta t/\Delta x$, for any basis polynomial degree $p > 0$; see page 191 of [13] and the references therein. Therefore, a different choice of time stepper will be needed to ensure both nonlinear and linear stability of the numerical scheme.

Proving that numerical schemes are TVD is difficult in general, so rather than seeking a new TVD scheme directly, we instead seek a scheme that will provably preserve the TVD properties of the FE method. Such schemes, referred to as *strong-stability-preserving* (SSP) methods, used in conjunction with a DG spatial discretization will, by definition, be TVD

under a time step restriction of the form

$$|c|\frac{\Delta t}{\Delta x} \leq \nu = \frac{1}{2}\mathcal{C}\,,$$

where $\mathcal{C}$ is commonly referred to as the SSP coefficient of the method.

The combined scheme must also satisfy a similar condition for linear stability:

$$|c|\frac{\Delta t}{\Delta x} \leq \mu(p, \mathcal{S}),$$

where μ is a constant that is a function of both the polynomial degree p of the DG spatial discretization and the region of absolute stability $\mathcal{S}$ of the time stepper (see Sect. 4 for the definition of $\mathcal{S}$ for MSRK methods). This gives the combined, general stability condition

$$|c|\frac{\Delta t}{\Delta x} \leq \kappa = \min\{\nu(\mathcal{C}), \mu(p, \mathcal{S})\}.$$

In [19], the value of κ for a DG spatial discretization and SSP-optimized RK methods was determined, and it was found that, in all cases $\mu(p, \mathcal{S}) < \nu(\mathcal{C})$. This motivated the construction of new SSP RK schemes with maximal μ, and therefore κ, when used with DG spatial discretizations [20]. Here, we extend the work of [19] by evaluating the linear stability properties of the SSP-optimized MSRK methods of [4] paired with DG spatial discretizations.

4 Linear Stability of MSRKDG Methods

In this section, we cover the linear stability properties of MSRK methods used in conjunction with DG spatial discretizations. For detailed discussion of the SSP properties of the MSRK methods used in this paper, see [4].

MSRK methods compute the solution at the end of a time step using multiple solution values from previous time steps, as well as a number of intermediate stage values within the current time step. Applied to an ODE of the form

$$\frac{du}{dt} = F(u)\,, \tag{7}$$

an r-step, s-stage MSRK method can be written

$$y_1^n = u^n\,, \tag{8}$$

$$y_i^n = \sum_{l=1}^{r} d_{il} u^{n-r+l} + \Delta t \sum_{l=1}^{r-1} \hat{a}_{il} F(u^{n-r+l}) + \Delta t \sum_{j=1}^{i-1} a_{ij} F(y_j^n)\,, \quad 2 \leq i \leq s\,, \tag{9}$$

$$u^{n+1} = \sum_{l=1}^{r} \theta_l u^{n-r+l} + \Delta t \sum_{l=1}^{r-1} \hat{b}_l F(u^{n-r+l}) + \Delta t \sum_{j=1}^{s} b_j F(y_j^n)\,, \tag{10}$$

where u^n and u^{n+1} are the solution values at the beginning and end of the current time step, respectively, u^{n-r+l} are the solution values from previous time steps, y_i^n are intermediate stage values, and d_{il}, a_{ij}, $\hat{a}_{il}$, θ_l, $\hat{b}_l$, and b_j are the coefficients of the particular MSRK method.

The linear stability of an MSRK method is analyzed by applying it to the scalar ODE

$$\frac{du}{dt} = \lambda u\,, \quad \lambda \in \mathbb{C}\,, \tag{11}$$

which results in a relation of the form

$$u^{n+1} = \sum_{l=1}^{r} Q_l(z) u^{n-r+l}$$

where $z = \lambda \Delta t$ and $Q_l(z)$ are polynomials with respect to z. The MSRK method is linearly stable if all roots of the corresponding stability polynomial

$$P(w; z) = w^k - \sum_{l=1}^{r} Q_l(z) w^{l-1},$$

lie within the unit circle in the complex plain [5]. That is, the method is stable if

$$|\omega| < 1, \quad \forall \omega \in W(z), \tag{12}$$

where $|\cdot|$ is the complex modulus and $W(z) = \{w \in \mathbb{C} : P(w; z) = 0\}$ is the set of roots of the stability polynomial. We define the region of absolute stability to be

$$\mathcal{S} = \{z \in \mathbb{C} : |\omega| < 1, \forall \omega \in W(z)\}. \tag{13}$$

The method is then stable as long as

$$\lambda \Delta t = z \in \mathcal{S}. \tag{14}$$

In the case where (11) is replaced with a matrix-vector equation of the form

$$\frac{d\mathbf{u}}{dt} = \mathbf{C}\mathbf{u},$$

condition (14) must hold for all $\lambda \in \Lambda$, where Λ is the set of eigenvalues of the constant matrix $\mathbf{C}$. We encounter such a case when analyzing the stability of the combined MSRKDG method by first applying a DG spatial discretization to the general hyperbolic conservation law (1) with flux function $f = cu$, which results in a system of linear equations of the form (5) with $\mathbf{L}(\mathbf{u}) = \mathbf{L}_h \mathbf{u}$, i.e.

$$\frac{d\mathbf{u}}{dt} = \mathbf{L}_h \mathbf{u},$$

where the subscript h denotes the dependence of $\mathbf{L}_h$ on the mesh spacing. Therefore the MSRKDG method is stable as long as condition (14) holds for all $\lambda \in \Lambda_{\mathbf{L}_h}$, where $\Lambda_{\mathbf{L}_h}$ is the set of eigenvalues of $\mathbf{L}_h$. For details on obtaining the eigenvalues of $\mathbf{L}_h$, see, for example, [16].

Noting that the region of absolute stability $\mathcal{S}$ is a property of the MSRK method alone and the values λ are dependent only upon the DG operator $\mathbf{L}_h$, we can plot $\mathcal{S}$ and the scaled eigenvalues $z = \lambda \Delta t$ for a useful illustration of the stability properties of the MSRKDG scheme. See Fig. 2 for an example plot of the stability region for an order two MSRK method with $r = 2$ steps and $s = 2$ stages. Within the stability region, the eigenvalues λ are plotted, scaled by the maximum stable Δt. Note that the $\lambda \Delta t$ points are all within the white-shaded stability region, implying that the method is linearly stable.

5 Methods for Determining Linear Stability Constraints

Two separate tests were performed to determine linear stability constraints for the combined MSRKDG schemes: a theoretical test, based upon condition (12), and a numerical test involving application of the MSRKDG scheme to solve a PDE. In both cases, a bisection algorithm,

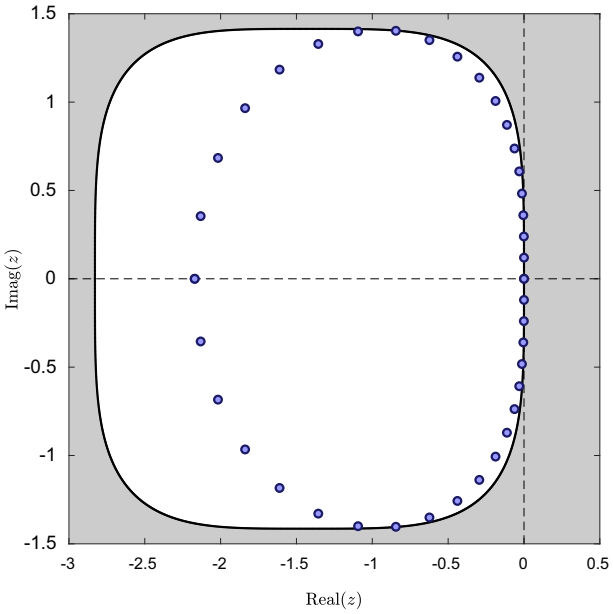

Fig. 2 The region of absolute stability for the SSP MSRK method of order two with $r = 2$ steps and $s = 2$ stages. The region of absolute stability is shown in white, with a black line marking the boundary of the region. Blue dots represent the eigenvalues of the DG spatial operator scaled by the maximum stable time step (Color figure online)

detailed in Algorithm 1, was used to arrive at an estimate for the linear stability constraint μ. The bisection algorithm begins by choosing initial bounds $\mu_{\min}$ and $\mu_{\max}$. Stability is then tested for a value of $\mu_{\text{bisect}} = (\mu_{\max} + \mu_{\min})/2$. If the method is found to be stable, $\mu_{\min}$ is set equal to μ_{bisect}; otherwise, the value of μ_{bisect} is set as the new $\mu_{\max}$. This process is repeated until $(\mu_{\max} - \mu_{\min})$ is less than the chosen tolerance $\epsilon = 1 \times 10^{-4}$. Once the tolerance is reached, the final estimate of the linear stability constraint is taken to be $\mu = \mu_{\min}$. In the results that follow, theoretical estimates of linear stability constraints are denoted μ_t, and numerical estimates are denoted μ_n.

Algorithm 1 Bisection procedure for determining estimates of μ.

$\mu_{\min} = 0.0$
$\mu_{\max} = 2.0$
while $(\mu_{\max} - \mu_{\min}) > \epsilon$ **do**
  $\mu_{\text{bisect}} = (\mu_{\max} + \mu_{\min})/2$
  Test for stability of RKDG scheme
  if stable **then**
    $\mu_{\min} \leftarrow \mu_{\text{bisect}}$
  else
    $\mu_{\max} \leftarrow \mu_{\text{bisect}}$
  end if
end while
return $\mu_{\min}$

5.1 Theoretical Stability Test

Theoretical tests for the stability of MSRKDG schemes were performed using the Schur–Cohn algorithm [23] as described in [2]. The procedure is detailed in Algorithm 2. The constant DG matrix $\mathbf{L}_h$ is pre-computed, and for each $\lambda \in \Lambda_{\mathbf{L}_h}$, given μ_{bisect} from the bisection procedure, the value of z is determined (for convenience, we choose $c = 1$ and uniform mesh spacing $h_j = \Delta x = 1$, giving $\Delta t = \mu_{\text{bisect}}$). The stability polynomial $P(z)$ of the particular MSRK method is constructed and evaluated using the value of z determined in the previous step. The Schur test begins by constructing the inverse polynomial $P^*(w) = w^r \overline{P}(w^{-1})$, where $\overline{P}$ is the complex conjugate of P. If the absolute value of $a = -P(0)/P^*(0)$ is greater than one, subject to a chosen tolerance $\varepsilon = 1 \times 10^{-12}$, there is at least one root of the stability polynomial lying outside the unit circle in the complex plane—that is, the MSRKDG method is linearly unstable for the given μ_{bisect}. Otherwise, if $|a| < 1 + \varepsilon$, no unstable roots have been detected and a new polynomial $P(w) = w^{-1}(P(w) + aP^*(w))$ is constructed and the process is repeated. The test ends when either an unstable root is detected or the polynomial P has been reduced to a constant. If the test ends without finding an unstable root for any $z = \lambda \Delta t$, the MSRKDG method is determined to be stable for the given μ_{bisect}. Once the bisection tolerance was reached, the theoretical stability constraint was recorded as $\mu_t = \mu_{\min}$.

Algorithm 2 Schur test for location of stability polynomial roots.

```
for λ ∈ Λ do
    z = λμ_bisect
    P(w) ← P(w; z)
    for j = r, r − 1, . . . , 1 do
        P*(w) ← w^j P̄(w^{−1})
        a ← −P(0)/P*(0)
        if |a| > 1 + ε then
            return stable = False
        end if
        P(w) ← w^{−1}(P(w) + aP*(w))
    end for
end for
return stable = True
```

5.2 Numerical Stability Test

Numerical stability constraints μ_n were determined by applying the MSRKDG method to the linear advection equation of the form (1), with $f(u) = cu$, where $c = 1$ is the constant advection speed. Domain boundaries are taken to be $x_L = -2.0$ and $x_R = 2.0$, and the initial condition is the Gaussian function $u_0(x) = \exp(-(x/0.25)^2)$. A constant mesh spacing $h_j = \Delta x = 1/8$ is used. Because of the smooth nature of the solution, no slope limiter was required for this test. Again, bisection was performed on the linear stability constraint, with Δt for the run determined according to μ_{bisect}. The problem was run to a final time of $T = 100$, and if the L^2 norm of the solution grew by more than 10^{-4} compared to the initial L^2 norm, the method was deemed unstable and we assigned $\mu_{\text{bisect}} = \mu_{\max}$. Once the bisection tolerance was reached, the numerical stability constraint was recorded as $\mu_n = \mu_{\min}$.

Table 1 Time step constraints for linear stability μ and strong-stability-preservation ν for SSP MSRK methods with greatest μ_{eff} for each order q

q	r	s	μ	ν
2	1	3	0.5882	1.0000
3	2	6	0.5358	1.8883
4	5	5	0.2642	1.2805
5	4	2	0.0249	0.3336
6	5	3	0.0500	0.3283
7	5	7	0.1054	1.0232
8	5	6	0.0676	0.6772
9	4	9	0.0661	0.3532
10	3	20	0.0944	0.4585

r and s denote the number of steps and stages, respectively, for the listed methods

6 Results

Linear stability constraint estimates μ_t and μ_n were found for existing SSP MSRK schemes paired with DG schemes of the same order; that is, the DG polynomial basis degree $p = r-1$. After determining μ_t and μ_n we define our final stability constraint estimate to be the minimum of the two, which in all cases is μ_t. Multi-stage methods require multiple computations of the DG spatial operator each time step, so, in order to provide a fair comparison between methods with various numbers of stages, we compute an effective stability constraint $\mu_{\text{eff}} = \mu/s$. Tables 2, 3, 4, 5, 6, 7, 8, 9 and 10 list the resulting μ_{eff} for all of the SSP-optimized MSRK methods, as well as any existing SSP-optimized Runge–Kutta (RK) or linear multistep (LM) methods; see, e.g. [15]. The greatest μ_{eff} for each order is bolded. Note that for the third order methods, four of the $s = 6$ methods have equal greatest $\mu_{\text{eff}} = 0.0893$; in this case, the method with the least number of steps is bolded as the "optimal" method due to its decreased storage requirements compared to the other methods with equal μ_{eff}.

The MSRK (or RK, in the case of $q = 2$) methods with greatest μ_{eff} for each order q are listed in Table 1, along with their corresponding linear and nonlinear stability constraints. Note that, for each of the listed methods, $\mu < \nu$. Indeed, we find that all methods we tested have a stricter condition for linear stability than for nonlinear stability. Note also that the methods of orders $q = 5$ and 6 have anomalously strict stability constraints. These are caused by a region of absolute stability $\mathcal{S}$ that poorly accommodates the shape of the scaled eigenvalues of the DG operator; see Sect. 6.1.

Also in Tables 2, 3, 4, 5, 6, 7, 8, 9 and 10, for each SSP MSRK method, the percent difference

$$\varsigma = \frac{\mu_n - \mu_t}{\mu_t}$$

between the μ_n and μ_t, relative to their average, is listed. Note that ς is positive in all cases, indicating that $\mu_t < \mu_n$. In most cases, numerical and theoretical stability constraints are in good agreement, with $\varsigma < 1\%$. The most notable exceptions are for methods of order 5, which in most cases have $\varsigma > 200\%$, and to a lesser extent, methods of order 6, which have ς up to about 70%. While performing stability tests, we found that the estimated μ for $q = 5$ and 6 was very sensitive to the tolerances chosen for the stability tests. This again appears to be caused by the shape of the stability regions for these methods; see the discussion in the following subsection.

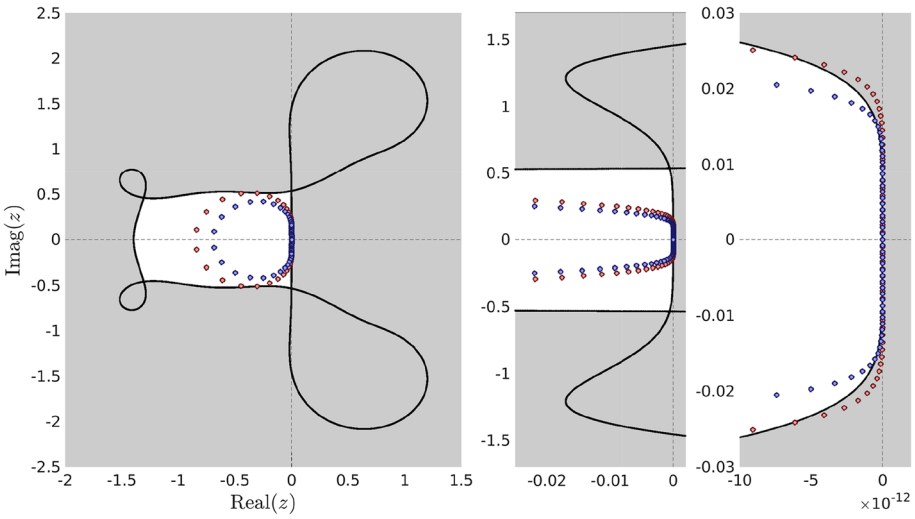

Fig. 3 Plot of the region of absolute stability (white shading, with black line boundary) of the MSRK method of order five with $r = 4$ steps and $s = 2$ stages, along with eigenvalues of the DG operator scaled by the maximum stable time step as determined according to μ_t (blue) and μ_n (red). The full stability region is shown on the left, with the middle plot zoomed to the imaginary axis to illustrate the curvature of the stability region boundary and the plot on the right zoomed to clearly show the points z_n falling outside the stability region (Color figure online)

6.1 On Strict Linear Stability Constraints for Fifth and Sixth Order Schemes

The strict stability constraints, as well as discrepancy between μ_t and μ_n for fifth and sixth order methods can be explained by examining their stability regions. As an example, in Fig. 3, we plot the region of absolute stability for the "optimal" fifth-order method listed in Table 1; that is, the method with $r = 4$ and $s = 2$. For this method, the percent difference between μ_t and μ_n is $\varsigma = 22.71\%$. Eigenvalues of the DG operator are plotted, scaled by the estimated maximum stable time steps according to both the theoretical (blue) and numerical (red) stability constraints. We refer to eigenvalues of the DG spatial operator scaled according to μ_t as z_t and those scaled according to μ_n as z_n.

We can see that, on a large scale, the z_n points seem to be a better fit to the stability region than the z_t points, with z_n points extending all the way to the boundary of the stability region near $z = -0.5 \pm 0.5i$. However, if we zoom in, we see that the boundary of the stability region curves toward the negative real side of the imaginary axis, and the curvature of the stability region boundary is such that there are z_n points lying outside the region of absolute stability near the imaginary axis, implying that the method is, in fact, theoretically unstable. This implies that the numerical test case has a certain built-in tolerance which allows for the theoretical stability constraint to be violated slightly without instabilities manifesting in the numerical stability test results. Of course, it should also be noted that we choose a tolerance ε for the theoretical stability test that, while apparently stricter than the built-in tolerance of the numerical test, may still be allowing some amount of instability. Nevertheless, as shown in the following section, the fifth and sixth order methods were found to converge in our test cases with Δt chosen according to the stability constraints presented in this paper.

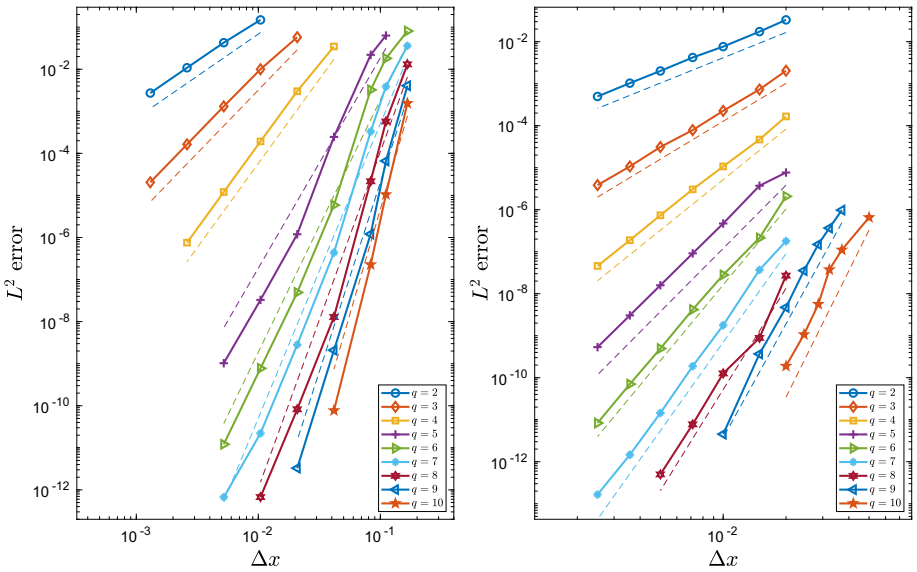

Fig. 4 Results of convergence tests for MSRK methods reported in Table 1. The left plot is of L^2 errors for the linear test case, and the right plot shows the L^2 error values for the nonlinear test case. Dashed lines in colors corresponding to the various orders q illustrate the slope of an error line with the desired order of convergence (Color figure online)

7 Test Cases

As an additional check on the stability of the SSP MSRKDG schemes, convergence tests were performed using Δt determined according to the reported stability constraints. Two separate tests were performed by applying the MSRKDG methods to solve a PDE of the form (1), one with a linear flux function $f(u) = cu$, and one with a nonlinear flux function $f(u) = (1/2)u^2$ (this is the classic inviscid Burgers' equation). To avoid any interference with high-order convergence, we did not use a slope limiter for these tests. In the case of the linear flux function, the domain was defined with $x_L = -2$ and $x_R = 2$, and the problem was run to a time of $T = 100$ with an initial condition $u_0(x) = \exp(-(x/0.25)^2)$. Several mesh refinements were performed, with uniform mesh spacing $h_j = \Delta x$ ranging from $\Delta x = 2/3$ to $\Delta x = 1/192$. The nonlinear test case was run on a domain with $x_L = 0$ and $x_R = 200$ with initial condition $x_0 = \sin(2\pi x/200)$. The problem was run to a final time of $T = 22$, well before the formation of a shock that occurs at $t = 33$. Again, several mesh refinements were performed, with constant mesh spacing varying from $\Delta x = 20$ to $\Delta x = 1/2$.

Results of the convergence tests for the methods with maximum μ_{eff} for each order are shown in Fig. 4. The L^2 error at the final time for each run is plotted, along with dashed lines illustrating the slope that should be observed for the expected order of convergence. All methods exhibit the expected order of convergence.

8 Conclusions

In this work, linear stability constraints were determined for SSP-optimized MSRK methods with DG spatial discretizations. The SSP MSRK methods studied in this paper allow us to

surpass the fourth order barrier of SSP RK schemes to achieve up to tenth order convergence. For each order $q = 2$ through 10, an "optimal" method was selected to minimize DG operator computations. All methods were found to converge at the desired order in application to both a linear and nonlinear PDE test case using the maximum stable time step as determined according to the results presented in this paper. For all methods, it was found that the linear stability constraint is more strict than the TVD constraint. This fact, combined with the observation that the stability regions for methods of orders $q = 5$ and 6 are poorly shaped to accommodate the DG operator eigenvalues, is strong motivation for the future development of SSP MSRK methods optimized specifically for DG spatial discretizations. We note that some of the previously developed DG-optimized RK methods of orders $q = 2$ and 3 have greater μ_{eff} than any of the SSP-optimized methods of the same order; see [20]. We expect that new DG-optimized time steppers with multiple steps could further improve upon those results.

Funding The authors would like to acknowledge funding from NSF Grants EAR-1520870 and ICER-1855047.

Data availability All data generated are included in the publication.

Declarations

Conflict of interest The authors declare no conflicts of interest with the material presented in this paper.

A Time Step Restrictions for SSP MSRK Methods with DG Spatial Discretizations

See Tables 2, 3, 4, 5, 6, 7, 8, 9 and 10.

Table 2 Effective stability constraints μ_{eff} and percent differences ς between numerical and theoretical stability constraint estimates for SSP RK, LM, and MSRK methods of order $q = 2$ with DG spatial discretization of degree $p = 1$

	$r = 1$	$r = 2$		$r = 3$		$r = 4$		$r = 5$	
	μ_{eff}	μ_{eff}	ς (%)	μ_{eff}	ς (%)	μ_{eff}	ς (%)	μ_{eff}	ς (%)
$s = 1$	...	...	–	0.1475	–	0.1710	–	0.1711	–
$s = 2$	0.1667	0.1809	0.25	0.1667	0.56	0.1508	0.69	0.1369	0.79
$s = 3$	**0.1961**	0.1677	0.60	0.1435	0.71	0.1251	0.87	0.1112	0.99
$s = 4$	0.1903	0.1508	0.64	0.1249	0.86	0.1071	1.00	0.0942	0.82
$s = 5$	0.1793	0.1363	0.76	0.1108	0.97	0.0940	0.74	0.0821	0.41
$s = 6$	0.1682	0.1243	0.87	0.0998	0.82	0.0840	0.41	0.0730	0.37
$s = 7$	0.1579	0.1144	0.90	0.0909	0.52	0.0762	0.34	0.0659	0.65
$s = 8$	0.1487	0.1061	0.77	0.0837	0.34	0.0698	0.50	0.0602	1.12

The maximum value of μ_{eff} is bolded

Table 3 Effective stability constraints μ_{eff} and percent differences ς between numerical and theoretical stability constraint estimates for SSP RK, LM, and MSRK methods of order $q = 3$ with DG spatial discretization of degree $p = 2$

	$r = 1$	$r = 2$		$r = 3$		$r = 4$		$r = 5$	
	μ_{eff}	μ_{eff}	ς (%)	μ_{eff}	ς (%)	μ_{eff}	ς (%)	μ_{eff}	ς (%)
$s = 1$	...	...	–	...	–	0.0522	–	0.0665	–
$s = 2$	...	0.0594	0.08	0.0705	0.27	0.0736	0.19	0.0736	0.19
$s = 3$	0.0699	0.0721	0.14	0.0765	0.18	0.0765	0.18	0.0765	0.18
$s = 4$	0.0766	0.0855	0.63	0.0855	0.63	0.0855	0.64	0.0855	0.62
$s = 5$	0.0812	0.0865	0.26	0.0865	0.26	0.0865	0.26	0.0865	0.26
$s = 6$	0.0807	**0.0893**	0.19	0.0893	0.19	0.0893	0.19	0.0893	0.19
$s = 7$	0.0810	0.0856	0.12	0.0856	0.12	0.0856	0.12	0.0856	0.12
$s = 8$	0.0806	0.0832	0.12	0.0832	0.12	0.0832	0.12	0.0832	0.12
$s = 9$	0.0000	0.0789	0.20	0.0806	0.20	0.0806	0.20	0.0806	0.20
$s = 10$	0.0000	0.0794	0.47	0.0794	0.47	0.0794	0.47	0.0794	0.47

The maximum value of μ_{eff} is bolded

Table 4 Effective stability constraints μ_{eff} and percent differences ς between numerical and theoretical stability constraint estimates for SSP RK, LM, and MSRK methods of order $q = 4$ with DG spatial discretization of degree $p = 3$

	$r = 1$	$r = 2$		$r = 3$		$r = 4$		$r = 5$	
	μ_{eff}	μ_{eff}	ς (%)	μ_{eff}	ς (%)	μ_{eff}	ς (%)	μ_{eff}	ς (%)
$s = 1$	...	...	–	...	–	...	–	0.0026	–
$s = 2$	...	...	–	0.0293	0.06	0.0361	0.04	0.0404	0.07
$s = 3$	...	0.0354	0.14	0.0442	0.11	0.0406	0.15	0.0431	0.17
$s = 4$	...	0.0444	0.13	0.0485	0.07	0.0512	0.04	0.0528	0.03
$s = 5$	0.0431	0.0468	0.13	0.0507	0.05	0.0520	0.06	**0.0528**	0.06
$s = 6$	0.0458	0.0482	0.16	0.0500	0.12	0.0502	0.06	0.0502	0.07
$s = 7$	0.0459	0.0473	0.11	0.0475	0.16	0.0476	0.13	0.0477	0.12
$s = 8$	0.0464	0.0480	0.17	0.0483	0.12	0.0484	0.11	0.0485	0.11
$s = 9$	...	0.0487	0.14	0.0499	0.24	0.0502	0.19	0.0502	0.17
$s = 10$	...	0.0487	0.21	0.0502	0.22	0.0502	0.21	0.0502	0.20

The maximum value of μ_{eff} is bolded

Table 5 Effective stability constraints μ_{eff} and percent differences ς between numerical and theoretical stability constraint estimates for SSP RK, LM, and MSRK methods of order $q = 5$ with DG spatial discretization of degree $p = 4$

	$r = 2$		$r = 3$		$r = 4$		$r = 5$	
	μ_{eff}	ς (%)	μ_{eff}	ς (%)	μ_{eff}	ς (%)	μ_{eff}	ς (%)
$s = 2$	...	–	...	–	**0.0125**	22.71	0.0117	104.34
$s = 3$	...	–	0.0116	86.04	0.0102	172.10	0.0097	209.65
$s = 4$	0.0108	118.43	0.0100	196.17	0.0099	211.09	0.0098	210.28
$s = 5$	0.0105	153.00	0.0099	192.44	0.0098	209.13	0.0099	212.23
$s = 6$	0.0099	196.22	0.0096	219.26	0.0096	220.25	0.0096	220.21
$s = 7$	0.0097	208.62	0.0096	211.41	0.0096	211.41	0.0096	211.41
$s = 8$	0.0093	242.66	0.0093	242.65	0.0093	242.65	0.0093	242.65
$s = 9$	0.0094	248.59	0.0095	244.46	0.0095	244.46	0.0095	244.46
$s = 10$	0.0083	248.70	0.0082	251.52	0.0082	249.69	0.0082	249.69

The maximum value of μ_{eff} is bolded

Table 6 Effective stability constraints μ_{eff} and percent differences ς between numerical and theoretical stability constraint estimates for SSP RK, LM, and MSRK methods of order $q = 6$ with DG spatial discretization of degree $p = 5$

	$r = 2$		$r = 3$		$r = 4$		$r = 5$	
	μ_{eff}	ς (%)	μ_{eff}	ς (%)	μ_{eff}	ς (%)	μ_{eff}	ς (%)
$s = 2$	...	–	...	–	...	–	0.0109	0.05
$s = 3$	...	–	0.0070	0.07	0.0137	0.09	**0.0167**	0.07
$s = 4$	...	–	0.0141	0.06	0.0157	16.31	0.0140	41.59
$s = 5$	...	–	0.0149	22.74	0.0142	37.87	0.0134	51.75
$s = 6$	0.0154	19.48	0.0145	34.49	0.0138	49.77	0.0131	67.05
$s = 7$	0.0141	1.72	0.0139	59.90	0.0141	53.84	0.0147	47.49
$s = 8$	0.0162	22.91	0.0123	45.74	0.0116	60.93	0.0112	69.12
$s = 9$	0.0144	33.28	0.0125	55.56	0.0122	60.30	0.0118	67.34
$s = 10$	0.0151	43.94	0.0133	53.47	0.0128	60.71	0.0124	63.80

The maximum value of μ_{eff} is bolded

Table 7 Effective stability constraints μ_{eff} and percent differences ς between numerical and theoretical stability constraint estimates for SSP RK, LM, and MSRK methods of order $q = 7$ with DG spatial discretization of degree $p = 6$

	$r = 2$		$r = 3$		$r = 4$		$r = 5$	
	μ_{eff}	ς (%)	μ_{eff}	ς (%)	μ_{eff}	ς (%)	μ_{eff}	ς (%)
$s = 3$	...	–	...	–	...	–	0.0092	0.03
$s = 4$	...	–	...	–	0.0024	0.14	0.0132	0.10
$s = 5$	...	–	0.0070	0.10	0.0131	0.05	0.0145	0.04
$s = 6$	...	–	0.0100	0.03	0.0145	0.11	0.0150	0.05
$s = 7$	...	–	0.0138	0.09	0.0145	0.05	**0.0151**	0.07
$s = 8$	0.0106	0.04	0.0127	0.16	0.0147	0.03	0.0132	0.10
$s = 9$	0.0121	0.02	0.0142	0.09	0.0141	0.10	0.0141	0.09
$s = 10$	0.0123	0.07	0.0150	0.03	0.0148	0.06	0.0148	0.04

The maximum value of μ_{eff} is bolded

Table 8 Effective stability constraints μ_{eff} and percent differences ς between numerical and theoretical stability constraint estimates for SSP RK, LM, and MSRK methods of order $q = 8$ with DG spatial discretization of degree $p = 7$

	$r = 3$		$r = 4$		$r = 5$	
	μ_{eff}	ς (%)	μ_{eff}	ς (%)	μ_{eff}	ς (%)
$s = 5$	...	–	0.0051	0.14	0.0065	0.11
$s = 6$	...	–	0.0063	0.11	**0.0113**	0.06
$s = 7$	...	–	0.0057	0.08	0.0073	0.12
$s = 8$	0.0083	0.06	0.0066	0.08	0.0079	0.10
$s = 9$	0.0082	0.04	0.0087	0.11	0.0096	0.09
$s = 10$	0.0081	0.07	0.0090	0.08	0.0096	0.09

The maximum value of μ_{eff} is bolded

Table 9 Effective stability constraints μ_{eff} and percent differences ς between numerical and theoretical stability constraint estimates for SSP RK, LM, and MSRK methods of order $q = 9$ with DG spatial discretization of degree $p = 8$

	$r = 3$		$r = 4$		$r = 5$	
	μ_{eff}	ς (%)	μ_{eff}	ς (%)	μ_{eff}	ς (%)
$s = 8$	...	–	0.0052	0.03	...	–
$s = 9$	...	–	**0.0074**	0.03	0.0067	0.14
$s = 10$	0.0067	0.03	...	–	...	–

The maximum value of μ_{eff} is bolded

Table 10 Effective stability constraints μ_{eff} and percent differences ς between numerical and theoretical stability constraint estimates for SSP RK, LM, and MSRK methods of order $q = 10$ with DG spatial discretization of degree $p = 9$

	$r = 3$		$r = 6$	
	μ_{eff}	ς (%)	μ_{eff}	ς (%)
$s = 9$	...	–	0.0024	0.08
$s = 10$	**0.0047**	0.03	...	–

The maximum value of μ_{eff} is bolded

References

1. Aizinger, V., Dawson, C., Cockburn, B., Castillo, P.: The local discontinuous Galerkin method for contaminant transport. Adv. Water Resour. **24**, 73–87 (2001)
2. Benedir, M.: On the root distribution of general polynomials with respect to the unit circle. Signal Process. **53**, 75–82 (1995)
3. Biswas, R., Devine, K.D., Flaherty, J.: Parallel, adaptive finite element methods for conservation laws. Appl. Numer. Math. **14**, 255–283 (1994)
4. Bresten, C., Gottlieb, S., Grant, Z., Higgs, D., Ketcheson, D., Németh, A.: Explicit strong stability preserving multistep Runge–Kutta methods. Math. Comput. **86**(304), 747–769 (2017)
5. Butcher, J.C.: Numerical Methods for Ordinary Differential Equations, 2nd edn. Wiley, Hoboken (2008)
6. Chapelier, J.B., de la Llave Plata, M., Renac, F., Lamballais, E.: Evaluation of a high-order discontinuous Galerkin method for the DNS of turbulent flows. Comput. Fluids **95**, 210–226 (2014)
7. Cheng, Y., Li, F., Qiu, J., Xu, L.: Positivity-preserving DG and central DG methods for ideal MHD equations. J. Comput. Phys. **238**, 255–280 (2013)
8. Cockburn, B., Hou, S., Shu, C.W.: The Runge–Kutta local projection discontinuous Galerkin finite element method for conservation laws IV: the multidimensional case. Math. Comput. **54**(190), 545–581 (1990)
9. Cockburn, B., Hou, S., Shu, C.W.: The Runge–Kutta discontinuous Galerkin method for conservation laws V: multidimensional systems. J. Comput. Phys. **141**, 199–224 (1998)
10. Cockburn, B., Lin, S.Y., Shu, C.W.: TVB Runge–Kutta local projection discontinuous Galerkin finite element method for conservation laws III: one-dimensional systems. J. Comput. Phys. **84**, 90–113 (1989)
11. Cockburn, B., Shu, C.W.: The Runge–Kutta local projection P^1-discontinuous Galerkin finite element method for scalar conservation laws. Math. Modell. Numer. Anal. **25**(3), 337–361 (1989)
12. Cockburn, B., Shu, C.W.: TVB Runge–Kutta local projection discontinuous Galerkin finite element method for scalar conservation laws II: general framework. Math. Comput. **52**, 411–435 (1989)
13. Cockburn, B., Shu, C.W.: Runge–Kutta discontinuous Galerkin methods for convection-dominated problems. J. Sci. Comput. **16**(3), 173–261 (2001)
14. Eskilsson, C., Sherwin, S.J.: A triangular spectral hp discontinuous Galerkin method for modelling 2d shallow water equations. Eng. Comput. **45**, 605–623 (2004)
15. Gottlieb, S., Ketcheson, D., Shu, C.W.: Strong Stability Preserving Runge–Kutta and Multistep Time Discretizations. World Scientific, Singapore (2011)
16. Krivodonova, L., Qin, R.: An analysis of the spectrum of the discontinuous Galerkin method. Appl. Numer. Math. **64**, 1–18 (2013)
17. Kubatko, E.J., Bunya, S., Dawson, C., Westerink, J.J.: Dynamic p-adaptive Runge–Kutta discontinuous Galerkin methods for the shallow water equations. Comput. Methods Appl. Mech. Eng. **198**, 1766–1774 (2009)
18. Kubatko, E.J., Westerink, J.J., Dawson, C.: hp discontinuous Galerkin methods for advection dominated problems in shallow water flow. Comput. Methods Appl. Mech. Eng. **196**, 437–451 (2006)
19. Kubatko, E.J., Westerink, J.J., Dawson, C.: Semidiscrete discontinuous Galerkin methods and stage exceeding order strong stability preserving Runge–Kutta time discretizations. J. Comput. Phys. **222**, 832–848 (2007)
20. Kubatko, E.J., Yeager, B.A.: Optimal strong-stability-preserving Runge–Kutta time discretizations for discontinuous Galerkin methods. J. Sci. Comput. **60**, 313–344 (2014)
21. Mirabito, C., Dawson, C., Kubatko, E.J., Westerink, J.J., Bunya, S.: Implementation of a discontinuous Galerkin morphological model on two-dimensional unstructured meshes. Comput. Methods Appl. Mech. Eng. **200**, 189–207 (2011)
22. Puelza, C., Čanić, S., Rivière, B., Rusin, C.G.: Comparison of reduced models for blood flow using Runge–Kutta discontinuous Galerkin methods. Appl. Numer. Math. **115**, 114–141 (2017)
23. Schur, J.: Über potenzreihen, die im innern des einheitskreises beschränkt sind. Journal für die reine und angewandte Mathematik **1917**(147), 205–232 (1917)
24. Shu, C.W., Osher, S.: Efficient implementation of essentially non-oscillatory shock-capturing schemes. J. Comput. Phys. **77**, 439–471 (1988)
25. Sun, T., Qiu, J.: LWDG method for a multi-class traffic flow model on an inhomogeneous highway. Adv. Appl. Math. Mech. **1**(3), 438–450 (2009)
26. Trahan, C.J., Dawson, C.: Local time-stepping in Runge–Kutta discontinuous Galerkin finite element methods applied to the shallow-water equations. Comput. Methods Appl. Mech. Eng. **217**, 139–152 (2012)
27. Xing, Y., Shu, C.W.: High order well-balanced finite volume WENO schemes and discontinuous Galerkin methods for a class of hyperbolic systems with source terms. J. Comput. Phys. **214**, 567–598 (2010)

28. Xing, Y., Zhang, X., Shu, C.W.: Positivity-preserving high order well-balanced discontinuous Galerkin methods for the shallow water equations. Adv. Water Resour. **33**, 1476–1493 (2010)